CRYSTAL GROWTH & DESIGN

pubs.acs.org/crystal

Article

Combining Sodium Profen Salts with Carbohydrates through Ionic Cocrystallization

Published as part of Crystal Growth & Design special issue "Design of Crystals via Crystallization Processes".

Ting Wen, Koen Robeyns, Nikolay Tumanov, Johan Wouters, Daniel M. Baier, Tongtong Wang, Songyang Miao, Xiang Liu, Guangxu Sun, Tom Leyssens,* and Fucheng Leng*

Cite This: *Cryst. Growth Des.* 2025, 25, 7208−7215

Read Online

ACCESS | Metrics & More | Article Recommendations | Supporting Information

ABSTRACT: Crystal engineering techniques that incorporate active pharmaceutical ingredients with sweetening agents present an effective methodology for mitigating the unpleasant taste characteristics of pharmaceutical compounds. Until now, carbohydrates, the natural and most common sweeteners, have rarely been used in taste masking through crystal engineering, probably due to their inability to form salt or unfavorable behavior in cocrystallization. In this study, profens, a series of popular anti-inflammatory drugs that could not be combined with carbohydrates, were transformed into their corresponding sodium salt forms and successfully combined with various carbohydrates through an ionic cocrystallization process, yielding several ionic cocrystals with a similar sandwich-like layered structure. Surprisingly, ionic cocrystallization with xylitol greatly reduced the hygroscopicity of sodium Profen salts. All three sodium Profen-xylitol ionic cocrystals exhibit anhydrous forms with minimal water absorption even under high relative humidity. This study highlights the potential of using carbohydrates as universal coformers with potential future application in taste masking, as well as reducing hygroscopicity issues of pharmaceutical sodium salts, providing valuable insights for drug formulation and stability improvement.

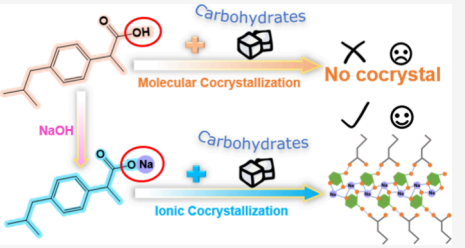

Downloaded via UNIV CATHOLIQUE DE LOUVAIN on January 23, 2026 at 10:33:39 (UTC).
See https://pubs.acs.org/sharingguidelines for options on how to legitimately share published articles.

INTRODUCTION

Profens, a class of nonsteroidal anti-inflammatory drugs (NSAIDs), are commonly used for pain relief, fever reduction, and inflammation management.[1] However, their unpleasant taste profile may present compliance challenges in clinical settings, particularly in pediatric applications.[2−4] Several methods have been developed for taste masking, including the utilization of flavoring agents and bitter inhibitors to block taste transmission, as well as cyclodextrins, ion exchange resins, polymer coating, and microencapsulation to prevent the release of the unpleasant taste.[5−10]

The crystal engineering method is also considered as an attractive taste masking approach, as it could mask taste and alter the physical properties of pharmaceutical compounds easily without changing the original structure of the pharmaceutical molecule.[11,12] Traditional crystal engineering methods for taste masking focus on combining artificial sweeteners, such as saccharin and sucralose with pharmaceutical molecules through cocrystallization or salt formation.[13−21] However, the most common and popular sweeteners, carbohydrates have been overlooked in this area for a long time. Carbohydrates, generally regarded as safe (GRAS) food additives by the FDA, are neutral and inexpensive, with their inherent sweetness effectively masking the bitterness of drugs and potentially increasing their solubility.[22−25] The long-standing neglect of carbohydrates in this area may be attributed to their inability to form salts and low success toward cocrystal formation. Indeed, until now, only a very limited number of carbohydrate molecular cocrystals have been reported.[24,26] However, ionic cocrystals (ICCs), normally defined as solids composed of neutral organic molecules and salts in defined stoichiometric ratios, have emerged as a new class of crystalline materials in crystal engineering and pharmaceutical development, offering a potential pathway for molecules that are difficult to form molecular cocrystals.[27] Notably, carbohydrates exhibited remarkable activity in ionic cocrystallization. For example, some inorganic salts, such as alkali metal halide salts and alkaline earth metal halide salts, showed great potential in combining with various carbohydrates like D-ribose, D-glucose, and D-sucrose.[28−34] Furthermore, recent research studies have demonstrated that pharmaceutical sodium salts, including sodium naproxen and sodium loxoprofen, can be effectively combined with carbohydrates to achieve enhanced physicochemical properties.[35,36]

Received: May 27, 2025
Revised: August 11, 2025
Accepted: August 12, 2025
Published: August 18, 2025

ACS Publications

© 2025 American Chemical Society

https://doi.org/10.1021/acs.cgd.5c00762
Cryst. Growth Des. 2025, 25, 7208−7215

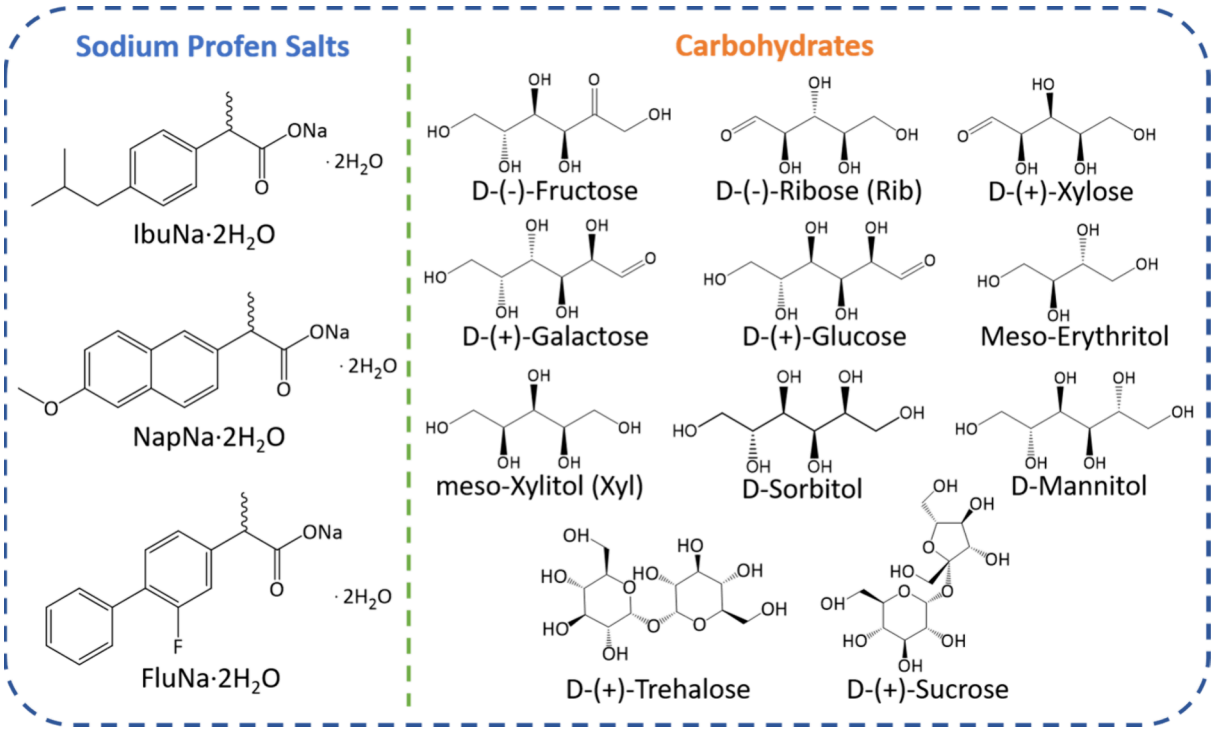

Figure 1. Chemical structures of 3 sodium Profen salts and 11 carbohydrates.

In this work, three profens and 11 carbohydrates were selected for a systematic cocrystal screening. Whereas none of the parent profens could be combined with the carbohydrates, their sodium salt forms demonstrated affinity toward specific carbohydrates such as D-ribose (Rib), D-fructose, and xylitol (Xyl). The structures of several ICCs were studied in detail using single-crystal X-ray diffraction and electron diffraction. Interestingly, despite some molecular differences between profens, all ICCs show a very similar packing mode, leading to a sandwich-like, layer-by-layer structure, in which carbohydrates coordinated with Na^+ cations form two-dimensional layers, while the profens are located between these layers. Notably, the cocrystals between sodium profens and Xyl exhibit an anhydrous form with minimal water adsorption, even under high humidity conditions.

EXPERIMENTAL SECTION

Materials. Racemic sodium ibuprofen dihydrate (IbuNa·$2H_2O$) was purchased from Merck. Racemic naproxen (Nap) and flurbiprofen (Flu) were bought from Tokyo Chemical Industry Co., Ltd., which are further converted to their corresponding sodium salt forms through reacting with NaOH obtained from Fisher Scientific. Three sodium Profen salts were examined by thermal analysis to confirm their hydrate forms (Figure S1). D-(−)-fructose anhydrous, D-(−)-ribose (Rib), D-(+)-xylose, D-(+)-galactose anhydrous, D-(+)-glucose anhydrous, D-(+)-trehalose anhydrous, D-(+)-sucrose, meso-erythritol, xylitol (Xyl), D-sorbitol, and D-mannitol were obtained from Tokyo Chemical Industry Co., Ltd. All solvents were employed as obtained without further processing. All molecular structures studied here are shown in Figure 1.

Methods. *Screening Experiments.* 0.5 mmol of sodium Profen salt and an equimolar amount of carbohydrate were placed in an Eppendorf tube, along with 5 μL of EtOH and three stainless steel balls (Ø 3 mm). Then the grinding process was performed using a RETSCH Mixer Mill MM 400 at a frequency of 30 Hz for 60 min. Subsequently, the Powder X-ray Diffraction (PXRD) patterns of the ground powder were compared with those of starting materials to identify any new peaks.

Preparation of IbuNa-Rib·H_2O and NapNa-Rib·0.35H_2O. 0.5 mmol of sodium Profen salt and 0.5 mmol of Rib were suspended in 3 mL of EtOH for 48 h and then filtrated to get the powder.

Preparation of NapNa-Rib·H_2O. 0.5 mmol of NapNa·$2H_2O$ and 0.5 mmol of Rib were suspended in 3 mL of ACN for 48 h and then filtrated to get the powder.

Preparation of FluNa-Rib·H_2O. 0.1 mmol of FluNa·$2H_2O$ and 0.1 mmol of Rib were dissolved in 5 mL of MeOH and then slowly evaporated to get the powder.

Preparation of IbuNa-Xyl, NapNa-Xyl and FluNa-Xyl. 0.5 mmol of sodium Profen salt and 0.5 mmol of Xyl were suspended in 3 mL of EtOH for 48 h and then filtrated to get the powder.

Single Crystal Growth. Approximately 10 mg of the ground powder was dissolved in 3 mL of MeOH at 40 °C, then the solution was cooled to room temperature and evaporated slowly. The colorless single crystals of IbuNa-Rib·H_2O, IbuNa-Xyl, NapNa-Rib·0.35H_2O, NapNa-Xyl, and FluNa-Xyl were successfully obtained after a few days. For NapNa-Rib·H_2O and FluNa- Rib·H_2O, only powder could be obtained from the preparation method described above, thus structure determination was performed by microcrystal electron diffraction (micro-ED).

Analytical Techniques. *PXRD.* All PXRD patterns were acquired using a Bruker D8, which was equipped with a Cu Kα X-ray source (λ=1.5406 Å) operating at 40 kV and 30 mA. The diffraction data were collected over a 2θ range of 4−40° with a step size of 0.02°.

Variable Temperature Powder X-ray Diffraction (VT-PXRD). The thermal stability and phase transitions due to dehydration of ICCs were investigated using a Bruker D8 Discover which was equipped with a Cu Kα X-ray source (λ=1.5406 Å) operating at 40 kV and 30 mA. The diffraction data were collected over a 2θ range of 4−40° with a step size of 0.015°, and over a temperature range of 25 to 145 °C with temperature steps of 20 °C.

Differential Scanning Calorimetry (DSC). DSC analyses were performed using TA Instrument DSC2500, calibrated by indium. All ICC samples (3−6 mg) were weighed and loaded into aluminum Tzero pans with sealed lids. The measurements were conducted at

https://doi.org/10.1021/acs.cgd.5c00762
Cryst. Growth Des. 2025, 25, 7208−7215

temperatures ranging from 25 to 200 °C, with a heating rate of 10 °C/min, under nitrogen gas flowing at a constant rate of 50 mL/min.

Thermogravimetric Analysis (TGA). TGA analyses were conducted using a Mettler Toledo TGA/DSC 3+ instrument. All ICCs samples (5−10 mg) were weighed and then loaded into open aluminum oxide crucibles and heated from 25 to 300 °C at a heating rate of 10 °C/min under nitrogen.

Dynamic Vapor Sorption (DVS). The TA Q5000 was employed to measure DVS curves. Approximately 4 mg of the ICC powder was weighed into a quartz pan and dried at 70 °C/1% RH for 90 min, and then exposed to the following RH levels: 0−80% in 5% increments at 25 °C. At every stage, the powder mass was equilibrated (the change in mass was less than 0.01% for 15 min, maximum dwell time 90 min) before adjusting the RH.

Single-Crystal X-ray Diffraction (SCXRD). Diffraction data were obtained using a MAR345 image plate detector and Mo Kα radiation (λ=0.71073 Å) produced by an Incoatec IμS microfocus source. All the acquired data were integrated and reduced by CrysAlis^{Pro}. The structures were solved using the dual-space algorithm in SHELXT and further refined against F^2 using SHELXL.[37]

Microcrystal Electron Diffraction (micro-ED). Electron diffraction data were collected at a Thermo Scientific 200 kV Glacios Cryo-TEM with a Ceta-D detector or Ceta-S detector. During the data collection, the particle was continuously rotated from −40° to 40° at a speed of 1°/s. The exposure time for each diffraction frame was 0.5 s and 160 frames were collected from each sample particle. The electron dose rate was about 0.04 electrons·Å^{-2}·s^{-1} and the temperature during the experiments was controlled at 90 K. Thermo Scientific EPU-D was used for data collection. Diffraction data from each particle were indexed and reduced by XDS.[38] Then the data from multiple different particles were merged by XSCALE. The crystal structure was solved by SHELXT and refined by SHELXL.[37]

RESULTS AND DISCUSSION

Screening Results. Initially, three commonly used NSAIDs—ibuprofen, naproxen, and flurbiprofen were attempted to be combined with 11 selected carbohydrates, including ketoses, aldoses, and sugar alcohols, using a mechanochemical method. Unfortunately, no new peaks were identified in the PXRD patterns, demonstrating the inability of profens to combine with carbohydrates (Figure S2). Inspired by the well-reported success of ionic cocrystallization between carbohydrates and sodium salts, the same screening procedure was applied to the sodium salt forms of profens. The appearance of new peaks, after grinding, conclusively proves the formation of a series of cocrystals primarily (Table S1). In order to obtain pure bulk material, the slurry method was employed for further preparation and study, with the resulting PXRD patterns shown in Figure S3. Notably, despite slight structural differences among the three sodium Profen salts, they can all form ICCs with Rib, D-(−)-fructose and Xyl, demonstrating that ionic cocrystals also follow, to some extent, our previous finding in molecular cocrystals that two molecules having relatively similar chemical structures are likely to form cocrystals with identical coformers. In this study, we focus in greater detail on the ICCs formed by Rib and Xyl.

Sodium Profen-Carbohydrate ICCs. SCXRD and micro-ED studies on seven sodium Profen-carbohydrate (Rib or Xyl) ICCs demonstrated that all of them share almost the same sandwich-like, layer-by-layer structure (Figure 2), in which carbohydrate molecules and Na^+ cations form one-dimensional chains or two-dimensional networks through coordination bonds, with Profen anions situated between the layers through hydrogen bonding between Profen anions and outward-facing hydroxyl groups on the carbohydrate. Their carboxyl groups are oriented toward the carbohydrate-Na chains or networks.

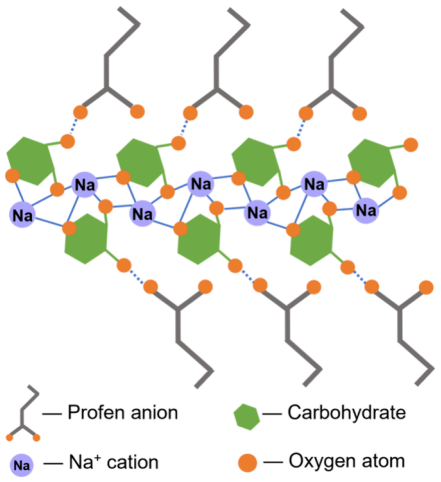

Figure 2. Schematic structure of sodium Profen-carbohydrate ICCs.

Structural Features of Sodium Profen-Rib ICCs. Thanks to the intrinsic chirality of Rib, all ICCs between Rib and three Profen sodium salts, including IbuNa-Rib·H_2O, NapNa-Rib·0.35H_2O, NapNa-Rib·H_2O, and FluNa-Rib·H_2O, crystallized in Sohncke space groups $P2_1$. However, approximately 50:50 R/S disorder was identified at the chiral carbon atoms of Profen anions, implying the formation of solid solutions, which inherently renders their application in the chiral resolution of profens by direct preferential crystallization impossible. The crystallographic data is shown in Table S2.

In all the structures, Rib molecules adopt a pyranose configuration, where the hydroxyl groups at positions 2′, 3′, and 4′ are oriented on the same side, forming a coordination pocket that can accommodate the Na^+ cation. Additionally, the bridging oxygen in the ring can form another coordination pocket with the hydroxyl groups at positions 2′ and 4′ to accommodate another Na^+ cation, allowing one Rib molecule to coordinate with two Na^+ cations simultaneously (Figure 3b,c).

In the case of IbuNa-Rib·H_2O and FluNa-Rib·H_2O, the bridging oxygen atom and the hydroxyl group at position 1′ form a bidentate ligand with the proximal Na^+ cation. However, this coordination mode is replaced by a monodentate interaction involving the hydroxyl group at position 3′ in NapNa-Rib·H_2O and NapNa-Rib·0.35H_2O (Figure 3c). To maintain structural stability, a water molecule occupies the available coordination site on the Na^+ cation. When the Na^+ cation is involved in one of these coordination environments, more than half of its coordination sphere remains unsatisfied. Consequently, an additional coordination pocket and other coordination modes complete the sphere, while they contain other Na^+ cations, forming an infinite one-dimensional coordination chain (Figure 3d).

The crystal packings of IbuNa-Rib·H_2O and NapNa-Rib·H_2O are displayed in Figure 4, NapNa-Rib·0.35H_2O and FluNa-Rib·H_2O are shown in Figure S4. Due to charge balance, Profen anions are situated between the one-dimensional chains formed by Na^+ cations and Rib molecules. On their hydrophilic side, the oxygen atoms of the carboxyl groups are connected through hydrogen bonds with the hydroxyl groups protruding from the Na-Rib coordination chain. Their hydrophobic sides form stacking arrangements at various angles through intermolecular forces like π-π stacking. It is worth noting that, although no coordination water is observed

https://doi.org/10.1021/acs.cgd.5c00762
Cryst. Growth Des. 2025, 25, 7208−7215

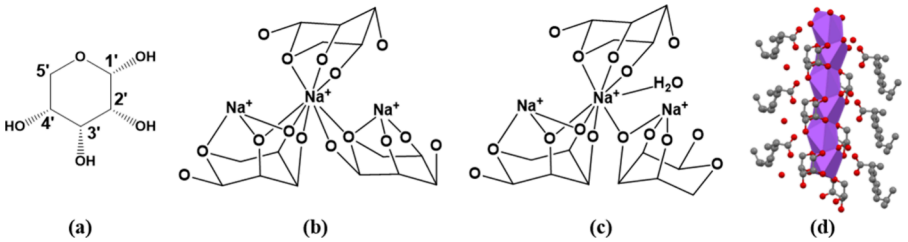

Figure 3. (a) Structure of α-D-ribopyranose; (b) coordination environment of Na^+ cations in IbuNa-Rib·H_2O and FluNa-Rib·H_2O; (c) coordination environment of Na^+ cations in NapNa-Rib·H_2O and NapNa-Rib·0.35H_2O; (d) one-dimensional coordination chain of IbuNa-Rib·H_2O. Carbon atoms are depicted in gray, oxygen atoms in red, sodium atoms in purple. Hydrogen atoms are omitted for clarity.

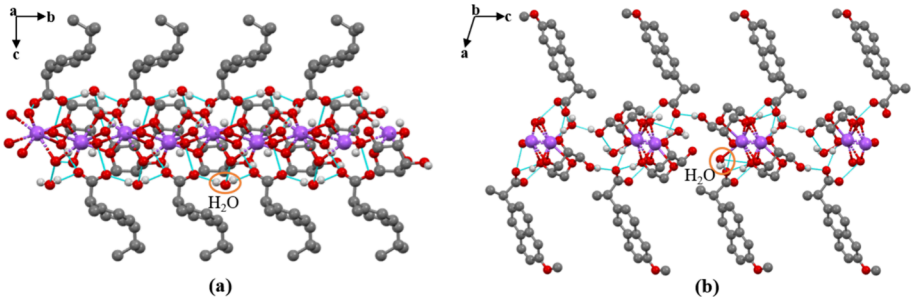

Figure 4. Crystal packing of (a) IbuNa-Rib·H_2O; (b) NapNa-Rib·H_2O. Coordination bonds are indicated by red dashed lines, hydrogen bonds in blue dashed lines. Hydrogen atoms that do not form hydrogen bonds are omitted.

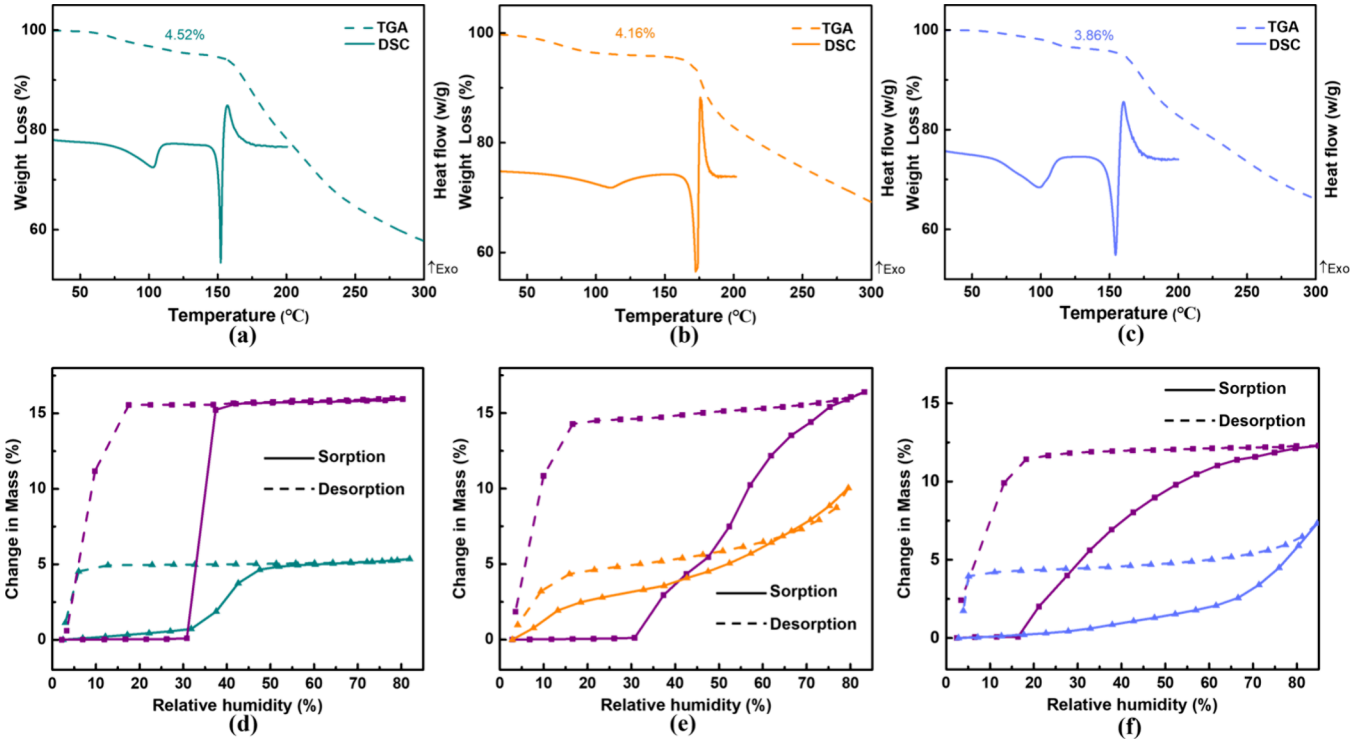

Figure 5. DSC and TGA results (top): (a) IbuNa-Rib·H_2O; (b) NapNa-Rib·H_2O; (c) FluNa-Rib·H_2O; DVS curves (bottom) of (d) IbuNa-Rib·H_2O; (e) NapNa-Rib·H_2O; (f) FluNa-Rib·H_2O. DVS curves of parent sodium Profen salts are depicted in purple lines.

in IbuNa-Rib·H_2O and FluNa-Rib·H_2O, water molecules are located between two Profen anions to bridge their carboxylic groups, which stabilizes the three-dimensional hydrogen bond network.

Thermal Characteristics. The DSC and TGA curves of the four sodium Profen-Rib ICCs exhibit similar thermal decomposition behavior, indicating comparable thermal stability. DSC curves of the three monohydrate ICCs (Figure 5, **top**) show broad endothermic peaks at approximately 100 °C due to dehydration. Correspondingly, their TGA profiles reveal weight losses of 4.52%, 4.16%, and 3.86% near 100 °C for IbuNa-Rib·H_2O, NapNa-Rib·H_2O, and FluNa-Rib·H_2O respectively, which is consistent with their theoretical weight losses calculated based on the crystal structures (4.54%, 4.28%, and 4.14%). Their phase transformation behavior is confirmed

https://doi.org/10.1021/acs.cgd.5c00762
Cryst. Growth Des. 2025, 25, 7208−7215

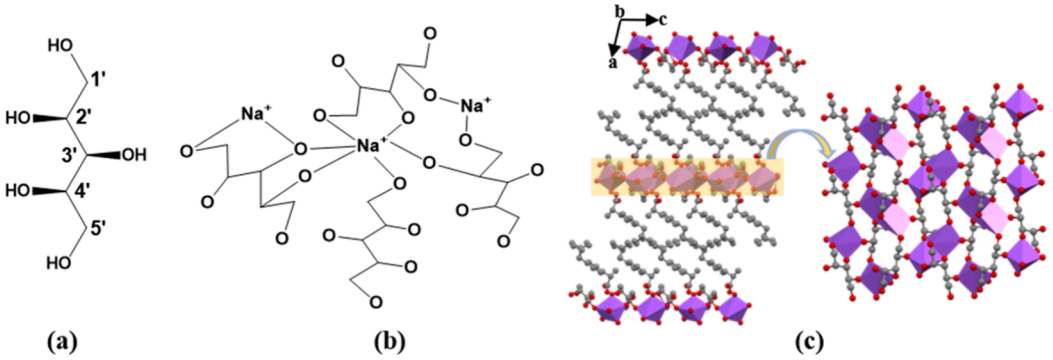

Figure 6. (a) Structure of xylitol; (b) coordination environment of Na^+ cations in sodium Profen-Xyl ICCs; (c) two-dimensional coordination network of IbuNa-Xyl. Carbon atoms are depicted in gray, oxygen atoms in red, sodium atoms in purple. Hydrogen atoms are omitted for clarity.

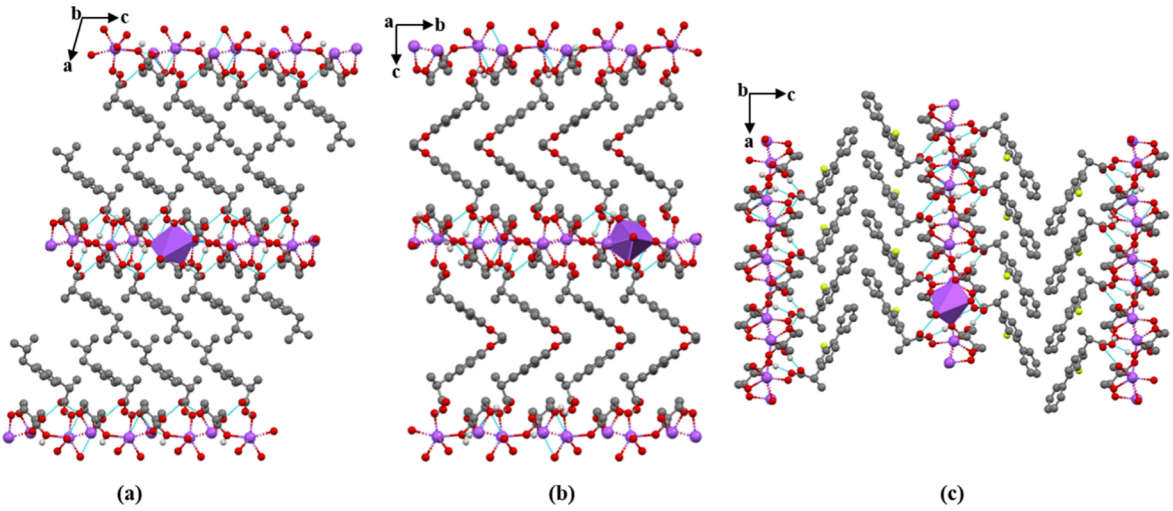

Figure 7. Crystal packing of (a) IbuNa-Xyl; (b) NapNa-Xyl; (c) FluNa-Xyl. Coordination bonds are indicated by red dashed lines, hydrogen bonds in blue dashed lines. Hydrogen atoms that do not form hydrogen bonds are omitted.

by VT-PXRD (Figure S5). The DSC and TGA results of NapNa-Rib·0.35H_2O are shown in Figure S6.

DVS experiments were performed to assess the hygroscopicity of these ICCs under various humidity conditions. The DVS curves of three parent sodium Profen salts and sodium Profen-Rib ICCs show typical water vapor sorption and desorption processes corresponding to hydrate forming systems. In the case of IbuNa-Rib, a clear 5% mass uptake at 35% RH corresponds to the formation of the monohydrated form, while this transformation occurs more gradually for NapNa-Rib and FluNa-Rib (Figure 5, **bottom**). The parent Profen salts exhibit similar behavior, where IbuNa forms a dihydrate at 35% RH, and NapNa shows a slower mass change due to the formation of multiple hydrate forms.[39,40] The PXRD patterns of the ICCs after drying and water vapor sorption processes are shown in Figure S7, with no evidence of polymorphic transformation observed for the anhydrous forms, all of which reverted to their original hydrated states upon exposure to moisture. The hysteresis observed in the DVS curves are indicative of differences in hydration and dehydration kinetics.

Structural Features of Sodium Profen-Xyl ICCs. Unlike Rib, Xyl is a meso compound, thus all three ICCs crystallize in a non-Sohncke space group. The crystallographic data is listed in Table S3. For IbuNa-Xyl and NapNa-Xyl, the asymmetric unit contains one Profen anion, one Na^+ cation and one open-chain Xyl molecule, whereas in FluNa-Xyl, two moiety formulas are present ($Z' = 2$). Apart from this, the environment of the Na^+ cations in the three ICCs exhibit significant similarity: each Na^+ cation has a coordination number of six, with coordination from six hydroxyl groups from four Xyl molecules, where two Xyl molecules act as bidentate ligands, while the remaining two function as monodentate ligands (Figure 6b). When Na^+ cations coordinate with hydroxyl groups from Xyl molecules, five hydroxyl groups can bridge multiple Na^+ cations in different directions due to the freely rotating chain-like structure of Xyl molecules and the even distribution of five hydroxyl groups, thereby forming a two-dimensional coordination network (Figure 6c). For the ICCs coordinated to the more rigid cyclic structure of Rib, the conformational restrictions only allow formation of one-dimensional chains.

The crystal packings of the three sodium Profen-Xyl ICCs also exhibit a layered structure, which is essentially similar to that of the ICCs coordinated with Rib, as shown in Figure 7. In addition, the overall structures of three sodium Profen-Xyl ICCs resemble each other, where Na^+ cations are interconnected by Xyl molecules through the same coordination network, and three different Profen anions are connected to Xyl molecules via the same hydrogen bond mode. The packing similarity between Ibu-Xyl and Flu-Xyl is quite high as shown by the crystal packing similarity module in Mercury,[41] which

https://doi.org/10.1021/acs.cgd.5c00762
Cryst. Growth Des. 2025, 25, 7208−7215

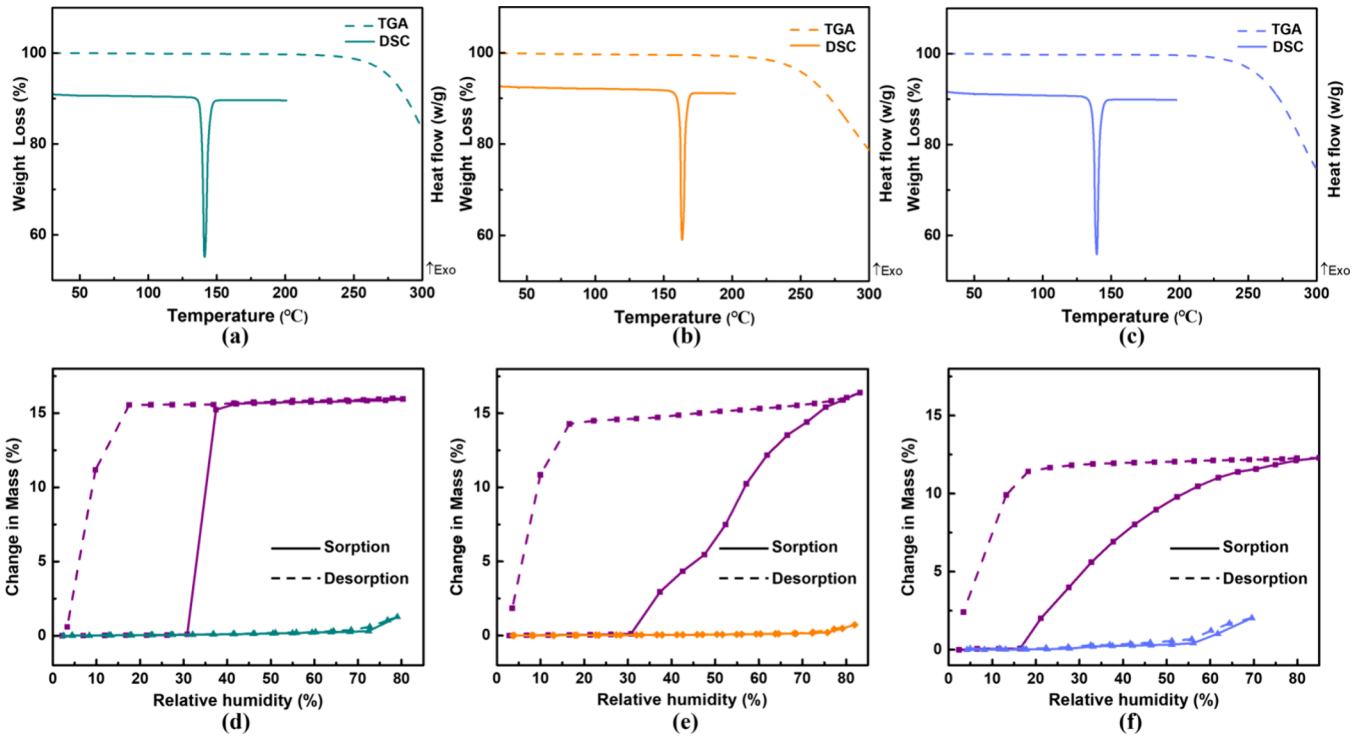

Figure 8. DSC and TGA results (top): (a) IbuNa-Xyl; (b) NapNa-Xyl; (c) FluNa-Xyl; DVS curves (bottom) of (d) IbuNa-Xyl; (e) NapNa-Xyl; (f) FluNa-Xyl. The DVS curves of parent sodium Profen salts are depicted in purple lines.

gives a RMSD deviation of 0.21 Å for 13 out of 20 molecules. The overlay of two crystal packings is shown in Figure S8.

Thermal Characteristics. All three sodium Profen-Xyl ICCs are found as anhydrates, and do not show any thermal events prior to their melting endotherm at 138.9 °C, 160.2 °C, and 136.3 °C, respectively (Figure 8, **top**). Moreover, their TGA curves illustrate that decomposition occurs only at approximately 250 °C, whereas the ICCs coordinated with Rib decompose immediately upon melting. This phenomenon may be attributed to the high thermal stability of Xyl. For ketoses or aldoses like fructose or ribose, caramelization readily occurs when the temperature exceeds 150 °C, leading to the decomposition of the samples.[42] However, Xyl, as a sugar alcohol, maintains excellent stability even at relatively high temperatures.[43]

Additionally, the three sodium Profen-Xyl ICCs show excellent humidity stability, in contrast to the ICCs coordinated with Rib, as evidenced by the absence of sudden mass changes and the uptake of only a minimal amount of surface water when the RH increases from 3.5% to 75%, suggesting that hydrate formation does not occur (Figure 8, **bottom**). The PXRD patterns of the ICCs after the sorption/desorption process also indicate the absence of any phase change (Figure S9). Given that pharmaceutical hydrates commonly face significant challenges during formulation, particularly in terms of stability and manufacturability, the strategy of ionic cocrystallization with Xyl emerges as a promising and innovative approach to effectively address these fundamental limitations.[44]

CONCLUSIONS

In this work, three sodium Profen salts were successfully combined with various carbohydrates, through ionic cocrystallization, yielding seven ICCs with identified structures. Although Rib and Xyl coordinate with Na^+ cations in different conformations, all ICCs share a sandwich-like layered structure. Moreover, resemblant structural characteristics were identified in three sodium Profen-Xyl ICCs. Interestingly, the ICCs coordinated with Rib are all hydrates, whereas those coordinated with Xyl are in anhydrous form and show excellent stability with respect to humidity, highlighting the critical role of coformers in preventing hydrate formation. This study not only underscores the potential of carbohydrates as effective coformers but also paves the way for carbohydrate-based ionic cocrystallization as a promising strategy for modifying the physicochemical properties of sodium Profen salts.

ASSOCIATED CONTENT

Supporting Information

The Supporting Information is available free of charge at https://pubs.acs.org/doi/10.1021/acs.cgd.5c00762.

Additional PXRD patterns, screening results, structures, and crystallographic data tables (PDF)

Accession Codes

Deposition Numbers 2454290−2454296 contain the supplementary crystallographic data for this paper. These data can be obtained free of charge via the joint Cambridge Crystallographic Data Centre (CCDC) and Fachinformationszentrum Karlsruhe Access Structures service. The supplementary crystallographic data for this paper is available in CCDC entries 2454290−2454296. These data can be accessed free of charge from The Cambridge Crystallographic Data Centre via www.ccdc.cam.ac.uk/structures.

https://doi.org/10.1021/acs.cgd.5c00762
Cryst. Growth Des. 2025, 25, 7208−7215

AUTHOR INFORMATION

Corresponding Authors

Tom Leyssens − *Institute of Condensed Matter and Nanosciences, Université catholique de Louvain, Louvain-La-Neuve 1348, Belgium;* orcid.org/0000-0001-7916-1373; Email: tom.leyssens@uclouvain.be

Fucheng Leng − *Food Science Building, University College Cork, Cork T12 K8AF, Ireland*; Email: fucheng.leng@ucc.ie

Authors

Ting Wen − *Institute of Condensed Matter and Nanosciences, Université catholique de Louvain, Louvain-La-Neuve 1348, Belgium*

Koen Robeyns − *Institute of Condensed Matter and Nanosciences, Université catholique de Louvain, Louvain-La-Neuve 1348, Belgium;* orcid.org/0000-0002-4763-4217

Nikolay Tumanov − *Chemistry Department, University of Namur, Namur 5000, Belgium;* orcid.org/0000-0001-6898-9036

Johan Wouters − *Chemistry Department, University of Namur, Namur 5000, Belgium;* orcid.org/0000-0002-4920-6857

Daniel M. Baier − *Institute of Condensed Matter and Nanosciences, Université catholique de Louvain, Louvain-La-Neuve 1348, Belgium*

Tongtong Wang − *XtalPi Inc, Shenzhen Jingtai Technology Co., Ltd., Shenzhen 518038, China*

Songyang Miao − *XtalPi Inc, Shenzhen Jingtai Technology Co., Ltd., Shenzhen 518038, China*

Xiang Liu − *XtalPi Inc, Shenzhen Jingtai Technology Co., Ltd., Shenzhen 518038, China*

Guangxu Sun − *XtalPi Inc, Shenzhen Jingtai Technology Co., Ltd., Shenzhen 518038, China*

Complete contact information is available at: https://pubs.acs.org/10.1021/acs.cgd.5c00762

Notes

The authors declare no competing financial interest.

ACKNOWLEDGMENTS

T.W. would like to thank the China Scholarship Council (CSC) for financial support. This paper is part of the COST action CA22107 − Bringing Experiment and Simulation together in Crystal Structure prediction.

REFERENCES

(1) Evans, A. M. Pharmacodynamics and pharmacokinetics of the profens: enantioselectivity, clinical implications, and special reference to S (+)-ibuprofen. *J. Clin. Pharmacol.* **1996**, *36*, 7S−15S.

(2) Breslin, P. A. S.; Gingrich, T. N.; Green, B. G. Ibuprofen as a Chemesthetic Stimulus: Evidence of a Novel Mechanism of Throat Irritation. *Chem. Senses* **2001**, *26* (1), 55−65.

(3) Milne, C. P.; Bruss, J. B. The economics of pediatric formulation development for off-patent drugs. *Clin. Ther.* **2008**, *30* (11), 2133−2145.

(4) Mennella, J. A.; Spector, A. C.; Reed, D. R.; Coldwell, S. E. The bad taste of medicines: overview of basic research on bitter taste. *Clin. Ther.* **2013**, *35* (8), 1225−1246.

(5) Breslin, P. A. S.; Beauchamp, G. K. Salt enhances flavour by suppressing bitterness. *Nature* **1997**, *387* (6633), 563−563.

(6) Ayenew, Z.; Puri, V.; Kumar, L.; Bansal, A. K. Trends in pharmaceutical taste masking technologies: a patent review. *Recent Pat. Drug Delivery Formul.* **2009**, *3* (1), 26−39.

(7) Yoshida, R.; Ohkuri, T.; Jyotaki, M.; Yasuo, T.; Horio, N.; Yasumatsu, K.; Sanematsu, K.; Shigemura, N.; Yamamoto, T.; Margolskee, R. F.; Ninomiya, Y. Endocannabinoids selectively enhance sweet taste. *Proc. Nat. Acad. Sci.* **2010**, *107* (2), 935−939.

(8) Wadhwa, J.; Puri, S. Taste masking: A novel approach for bitter and obnoxious drugs. *Int. J. Biopharm. Toxicol. Res.* **2011**, *1* (1), 47−60.

(9) Vummaneni, V.; Nagpal, D. Taste masking technologies: an overview and recent updates. *Int. J. Res. Pharm. Biomed. Sci.* **2012**, *3* (2), 510−524.

(10) Hu, S.; Liu, X.; Zhang, S.; Quan, D. An overview of taste-masking technologies: approaches, application, and assessment methods. *AAPS PharmSciTech* **2023**, *24* (2), 67.

(11) Yu, J.; Xie, J.; Xie, H.; Hu, Q.; Wu, Z.; Cai, X.; Guo, Z.; Lin, J.; Han, L.; Zhang, D. Strategies for Taste Masking of Orodispersible Dosage Forms: Time, Concentration, and Perception. *Mol. Pharmaceutics* **2022**, *19* (9), 3007−3025.

(12) An, J. P.; Wang, Y.; Munger, S. D.; Tang, X. A review on natural sweeteners, sweet taste modulators and bitter masking compounds: structure-activity strategies for the discovery of novel taste molecules. *Crit. Rev. Food Sci. Nutr.* **2025**, *65*, 2076−2099.

(13) Hou, X.; Feng, Y.; Zhang, P.; Wei, H.; Dang, L. Selective crystal growth of theophylline-saccharin cocrystal on self-assembled monolayer from incongruent system. *Cryst. Growth Des.* **2015**, *15* (10), 4918−4924.

(14) Arafa, M. F.; El-Gizawy, S. A.; Osman, M. A.; El Maghraby, G. M. Sucralose as co-crystal co-former for hydrochlorothiazide: development of oral disintegrating tablets. *Drug Dev. Ind. Pharm.* **2016**, *42* (8), 1225−1233.

(15) Kong, M.; Fu, X.; Li, J.; Li, J.; Chen, M.; Deng, Z.; Zhang, H. Sweet pharmaceutical salts of stanozolol with enhanced solubility and physical stability. *CrystEngComm* **2016**, *18* (45), 8739−8746.

(16) Arafa, M. F.; El-Gizawy, S. A.; Osman, M. A.; El Maghraby, G. M. Co-crystallization for enhanced dissolution rate of nateglinide: In vitro and in vivo evaluation. *J. Drug Delivery Sci. Technol.* **2017**, *38*, 9−17.

(17) Hyun, S.; Lee, B. J.; Abuzar, S. M.; Lee, S.; Joo, Y.; Hong, S.; Kang, H.; Kwon, K.; Velaga, S.; Hwang, S. Preparation, characterization, and evaluation of celecoxib eutectic mixtures with adipic acid/saccharin for improvement of wettability and dissolution rate. *Int. J. Pharm.* **2019**, *554*, 61−71.

(18) Soliman, I. I.; Kandil, S. M.; Abdou, E. M. Technology. Gabapentin−saccharin co-crystals with enhanced physicochemical properties and in vivo absorption formulated as oro-dispersible tablets. *Pharm. Dev. Technol.* **2020**, *25* (2), 227−236.

(19) Guan, D.; Xuan, B.; Wang, C.; Long, R.; Jiang, Y.; Mao, L.; Kang, J.; Wang, Z.; Chow, S. F.; Zhou, Q. J. P. Improving the physicochemical and biopharmaceutical properties of active pharmaceutical ingredients derived from traditional Chinese medicine through cocrystal engineering. *Pharmaceutics* **2021**, *13* (12), 2160.

(20) Liu, S.; Wang, C.; Chen, H.; Sun, C. Sweet sulfamethazine acesulfamate crystals with improved compaction property. *Cryst. Growth Des.* **2021**, *21* (2), 1077−1085.

(21) Leng, F.; Robeyns, K.; Leyssens, T.; Shemchuk, O. Combining racetams with a sweetener through complexation. *Cryst. Growth Des.* **2022**, *22* (5), 3016−3023.

(22) Mennella, J. A.; Reed, D. R.; Mathew, P. S.; Roberts, K. M.; Mansfield, C. J. "A spoonful of sugar helps the medicine go down": bitter masking by sucrose among children and adults. *Chem. Senses* **2015**, *40* (1), 17−25.

(23) Wagh, V. D.; Ghadlinge, S. V. Taste masking methods and techniques in oral pharmaceuticals: current perspectives. *J. Pharm. Res.* **2009**, *2* (6), 1049−1054.

(24) Nugroho, D.; Sugih, A. K. Preparation and characterization of highly water soluble curcumin−dextrose cocrystal. *Pure Appl. Chem.* **2018**, *7*, 140.

(25) Thakuria, R.; Delori, A.; Jones, W.; Lipert, M. P.; Roy, L.; Rodríguez-Hornedo, N. Pharmaceutical cocrystals and poorly soluble drugs. *Int. J. Pharm.* **2013**, *453* (1), 101−125.

(26) Palanisamy, V.; Sanphui, P.; Palanisamy, K.; Prakash, M.; Bansal, A. K. Design of ascorbic acid eutectic mixtures with sugars to inhibit oxidative degradation. *Front. Chem.* **2022**, *10*, No. 754269.
(27) Bolla, G.; Sarma, B.; Nangia, A. K. Crystal engineering of pharmaceutical cocrystals in the discovery and development of improved drugs. *Chem. Rev.* **2022**, *122* (13), 11514−11603.
(28) Duggirala, N. K.; Smith, A. J.; Wojtas, Ł.; Shytle, R. D.; Zaworotko, M. J. Physical stability enhancement and pharmacokinetics of a lithium ionic cocrystal with glucose. *Cryst. Growth Des.* **2014**, *14* (11), 6135−6142.
(29) Oertling, H.; Besnard, C.; Alzieu, T.; Wissenmeyer, M.; Vinay, C.; Mahieux, J.; Fumeaux, R. J. C. G. Design. Ionic cocrystals of sodium chloride with carbohydrates. *Cryst. Growth Des.* **2017**, *17* (1), 262−270.
(30) Jiang, Y.; Xue, J.; Wen, X.; Zhai, Y.; Yang, L.; Xu, Y.; Zhao, G.; Kou, K.; Liu, K.; Chen, J. E.; Wu, J. Sugar-metal ion interactions: The coordination behavior of cesium ion with lactose, d-arabinose and L-arabinose. *J. Mol. Struct.* **2016**, *1109*, 179−191.
(31) Hu, H.; Xue, J.; Wen, X.; Li, W.; Zhang, C.; Yang, L.; Xu, Y.; Zhao, G.; Bu, X.; Liu, K.; Chen, J.; Wu, J. Sugar−metal ion interactions: the complicated coordination structures of cesium ion with D-ribose and myo-inositol. *Inorg. Chem.* **2013**, *52* (22), 13132−13145.
(32) Cheng, H.; Wei, Y.; Wang, S.; Qiao, Q.; Heng, W.; Zhang, L.; Zhang, J.; Gao, Y.; Qian, S. Improving tabletability of excipients by metal-organic framework-based cocrystallization: A study of mannitol and $CaCl_2$. *Pharm. Res.* **2020**, *37* (7), 130.
(33) Xue, J.; Hua, X.; Li, W.; Yang, L.; Xu, Y.; Zhao, G.; Zhang, G.; Li, C.; Liu, K.; Chen, J.; Wu, J. Sugar−metal ion interactions: the coordination behaviors of lanthanum with erythritol. *Carbohydr. Res.* **2012**, *361*, 12−18.
(34) Allscher, T.; Kästele, X.; Kettenbach, G.; Klüfers, P.; Kunte, T. Sugar-alcohol complexes of Palladium (II): On the variable rigidity of open-chain carbohydrate ligands. *Chem.-Asian J.* **2007**, *2* (8), 1037−1045.
(35) Fujito, T.; Oshima, T.; Higashi, K.; Ueda, K.; Ito, M.; Masu, H.; Noguchi, S.; Moribe, K. J. C. G. Design. Salt Cocrystallization of loxoprofen sodium with sugar: reduction of the propensity for hydrate formation by forming a continuous one-dimensional chain structure of sodium and sugar. *Cryst. Growth Des.* **2022**, *22* (2), 1094−1103.
(36) Sovago, I.; Wang, W.; Qiu, D.; Raijada, D.; Rantanen, J.; Grohganz, H.; Rades, T.; Bond, A. D.; Löbmann, K. Properties of the sodium naproxen-lactose-tetrahydrate Co-crystal upon processing and storage. *Molecules* **2016**, *21* (4), 509.
(37) Sheldrick, G. M. Crystal structure refinement with SHELXL. *Cryst. Struct. Commun.* **2015**, *71* (1), 3−8.
(38) Kabsch, W. XDS. *Acta Crystallogr., Sect. D* **2010**, *66* (2), 125−132.
(39) Kim, Y. S.; Rousseau, R. W. Characterization and solid-state transformations of the pseudopolymorphic forms of sodium naproxen. *Cryst. Growth Des.* **2004**, *4* (6), 1211−1216.
(40) Censi, R.; Martena, V.; Hoti, E.; Malaj, L.; Di Martino, P. Sodium ibuprofen dihydrate and anhydrous: study of the dehydration and hydration mechanisms. *J. Therm. Anal. Calorim.* **2013**, *111*, 2009−2018.
(41) Macrae, C. F.; Bruno, I. J.; Chisholm, J. A.; Edgington, P. R.; McCabe, P.; Pidcock, E.; Rodriguez-Monge, L.; Taylor, R.; van de Streek, J.; Wood, P. A. Mercury CSD 2.0−new features for the visualization and investigation of crystal structures. *Appl. Crystallogr.* **2008**, *41* (2), 466−470.
(42) Jiang, B.; Liu, Y.; Bhandari, B.; Zhou, W. Impact of caramelization on the glass transition temperature of several caramelized sugars. Part I: chemical analyses. *J. Agric. Food Chem.* **2008**, *56* (13), 5138−5147.
(43) Varzakas, T.; Labropoulos, A.; Anestis, S. *Sweeteners: Nutritional Aspects, Applications, and Production Technology*; CRC Press: Boca Raton, 2012.
(44) Dhondale, M. R.; Thakor, P.; Nambiar, A. G.; Singh, M.; Agrawal, A. K.; Shastri, N. R.; Kumar, D. Co-crystallization approach to enhance the stability of moisture-sensitive drugs. *Pharmaceutics* **2023**, *15* (1), 189.

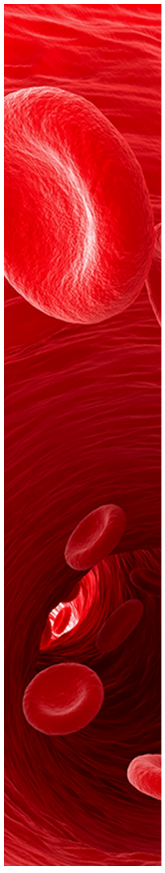
CAS BIOFINDER DISCOVERY PLATFORM™
CAS BIOFINDER HELPS YOU FIND YOUR NEXT BREAKTHROUGH FASTER
Navigate pathways, targets, and diseases with precision
Explore CAS BioFinder
CAS
A division of the American Chemical Society

https://doi.org/10.1021/acs.cgd.5c00762
Cryst. Growth Des. 2025, 25, 7208−7215